



Erythromycin loaded by tetrahedral framework nucleic acids are more antimicrobial sensitive against *Escherichia coli* (*E. coli*)

Yue Sun^a, Yuhao Liu^a, Bowen Zhang^a, Shirong Shi^a, Tao Zhang^a, Dan Zhao^a, Taoran Tian^a, Qirong Li^a, Yunfeng Lin^{a,b,*}

^a State Key Laboratory of Oral Diseases, National Clinical Research Center for Oral Diseases, West China Hospital of Stomatology, Sichuan University, Chengdu, 610041, China

^b College of Biomedical Engineering, Sichuan University, Chengdu, 610041, China

ARTICLE INFO

Keywords:

Tetrahedral framework nucleic acids
Drug delivery system
Escherichia coli
Drug penetration disorder
Erythromycin

ABSTRACT

Erythromycin is a commonly used broad-spectrum antibiotic, but resistance to this antibiotic makes its use less effective. Considerable efforts, beside finding alternatives, are needed to enhance its antimicrobial effect and stability against bacteria. Tetrahedral framework nucleic acids (tFNAs), a novel delivery vehicle with a three-dimensional nanostructure, have been studied as a carrying platform of antineoplastic drugs. In this study, the use of tFNAs in delivering erythromycin into *Escherichia coli* (*E. coli*) was investigated for the first time. The tFNAs vehicle increased the bacterial uptake of erythromycin and promoted membrane destabilization. Moreover, it increased the permeability of the bacterial cell wall, and reduced drug resistance by improving the movement of the drug across the membrane. The tFNAs-based delivery system enhanced the effects of erythromycin against *E. coli*. It may therefore provide an effective delivery vehicle for erythromycin in targeting antibiotic-resistant bacteria with thick cell wall.

1. Introduction

Erythromycin is a macrolide antibiotic that can irreversibly bind to the 50S subunit of bacterial ribosomes, resulting in the ribosomal inability to polymerize specific amino acid sequences during protein synthesis, by blocking the process of peptide transfer and mRNA transfer, and blocking the growth of the peptide chain, ultimately playing a bacteriostatic role [1,2]. The development of bacterial resistance is one of the greatest challenges to human health. Antibiotic resistance refers to the enhanced survival ability of bacteria in the presence of antibiotics and the reduced effectiveness of antibiotics against bacteria. Due to the incorrect use of drugs, drug-resistant strains have developed rapidly in the recent decades. According to clinical statistics, the drug resistance rate of pathogenic bacteria has reached 30–50%, and it increases by 5% every year [3,4]. The causes of erythromycin resistance mainly include [5–8]: 1. The N6 position in nucleotide A2058 is monomethylated or dimethylated. Methylation can interfere with the formation of hydrogen bonds, leading to a significant decrease in the affinity between

macrolides and ribosomal 50s subunits, resulting in the production of resistant strains; 2. the decrease in membrane permeability may lead to the decrease of drug uptake and accumulation, which may lead to drug resistance; 3. the induction of efflux pump may lead to a reduce intracellular concentration. (see Scheme 1)

Nucleic acids are important genetic materials in pathogenic microorganisms, which play a definite role in a series of important life phenomena, such as growth, heredity, and variation. Bacterial nucleic acids can be used to detect the pathogenicity and existence of drug-resistant genes in microorganisms [9,10]. Four single-stranded DNA (ssDNA) molecules self-assemble into tetrahedral configurations, forming Tetrahedral Framework Nucleic Acids (tFNAs), based on the highly specific complementary base pairing principle [11–13]. Previous studies showed that tFNAs have an excellent biocompatibility and a favorable ability to permeate bacterial and mammalian cells, that have been recognized as a promising delivery vehicle used in delivering drug molecules [14–19].

In recent years, the use of nanoparticles and other antibacterial materials to achieve bacterial control has attracted the attention of

Peer review under responsibility of KeAi Communications Co., Ltd.

* Corresponding author. State Key Laboratory of Oral Diseases, National Clinical Research Center for Oral Diseases, West China Hospital of Stomatology, Sichuan University, Chengdu, 610041, China.

E-mail address: yunfenglin@scu.edu.cn (Y. Lin).

<https://doi.org/10.1016/j.bioactmat.2020.12.027>

Received 2 December 2020; Received in revised form 25 December 2020; Accepted 28 December 2020

2452-199X/© 2021 The Authors. Production and hosting by Elsevier B.V. on behalf of KeAi Communications Co., Ltd. This is an open access article under the CC

BY-NC-ND license (<http://creativecommons.org/licenses/by-nc-nd/4.0/>).

researchers all over the world [20,21]. The application of nucleic acid materials in antibiotic research is mainly focused on target detection, and not on the improvement of antibacterial activity. To reduce the outflow of antibiotics from bacteria that are not sensitive to antibiotics, strengthening antibiotic delivery via endocytosis using tFNAs - could be an option [22–25]. In this study, we used tFNAs to deliver erythromycin (tFNAs-Ery), a commonly used broad-spectrum antibiotic, and evaluated its antibacterial properties against *Escherichia coli* (*E. coli*). Due to the strong transmembrane penetrative ability of tFNAs, tFNAs-Ery enable more erythromycin to enter the cell efficiently, and exert antibacterial properties more effectively compared with erythromycin alone. In addition, morphological observation revealed that even under the same erythromycin concentration, erythromycin transported using tFNAs did more damage to the bacterial membrane structure than did free erythromycin. tFNAs-Ery was more lethal than free erythromycin, possibly due to the changes in the cell membrane permeability made by tFNAs which allowed for an increased drug penetration.

2. Material and methods

2.1. Synthesis of tFNAs and drug loading

The specific synthesis details of tFNAs can be seen in previous research reports [26–28]. S1–S4 single DNA strands -Table 1 showed the sequence of bases for each strand of DNA. To form tFNAs-Ery, erythromycin solution (different content: 4000, 2000, 1000, 500 and 250 µg) was incubated with tFNAs (100 nM) at room temperature for 24 h, and then centrifuged at 10 000 rpm for 10 min with a 15KD ultrafiltration centrifuge tube to remove unloaded drug molecules and single strand of DNA. The loading efficiency of erythromycin into tFNAs was analyzed with UV-vis spectroscopy (U-3900H, HITACHI, JAPAN) to detect erythromycin absorbance peak at 236 nm. According to the content reflected by the peak area, the loaded drug content was calculated

(Table 2). The loading efficiency of erythromycin into tFNAs can be calculated as follows:

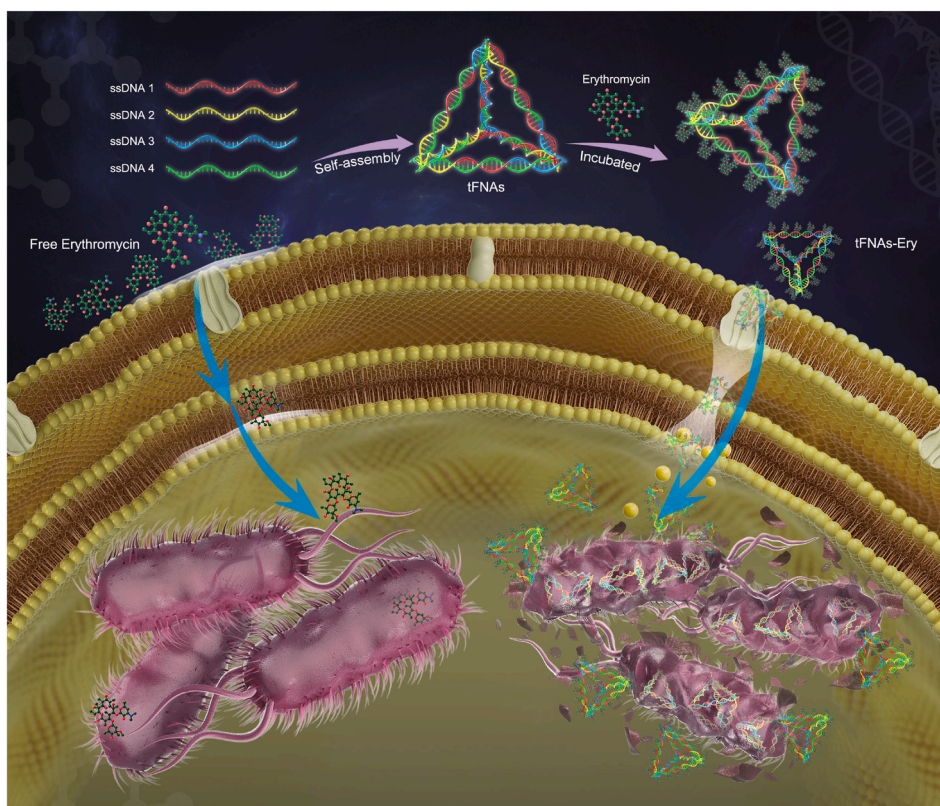
$$\text{Loading efficiency} = \frac{\text{Total drug} - \text{Free drug}}{\text{Total drug}} \times 100\%$$

2.2. Identification of the successfully synthesized tFNAs and tFNAs-Ery

For verification of tFNAs, 8% polyacrylamide gel electrophoresis (PAGE) was used to measure the molecular weights of four ssDNAs and tFNAs, Transmission electron microscopy (TEM, Libra200, Zeiss, German) and Atomic force microscopy (AFM, SPM-9700 instrument, Shimadzu, Kyoto, Japan) was performed for morphological structural observation of tFNAs and tFNAs-Ery. The hydrodynamic sizes and zeta potentials of tFNAs, erythromycin and tFNAs-Ery were measured using a Zeta sizer Nano-ZS (Malvern Instruments, England).

2.3. Cytotoxicity assay

HUVECs and L929 were purchased from the American Type Culture Collection (ATCC®CRL1730™). HUVECs and L929 cells was cultured in high-glucose DMEM (0.1 mM non-essential amino acids, 4 mM L-glutamine, 10% FBS and 1% penicillin-streptomycin antibiotics) and RPMI-1640 culture medium (10% FBS and 1% penicillin-streptomycin antibiotics), respectively. HUVECs and L929 cells were seeded in a 96-well plate (5000 per well) and incubated with tFNAs (100, 200, 250, 500 and 750 nM) and (tFNAs-Ery 5, 50, 500 µg/mL), respectively, for 24 h and 48 h. The changes in proliferation of HUVECs and L929 cells was detected with the cell counting kit-8 (CCK-8; Dojindo, Japan). Specifically, 100 µL medium was mixed with 10 µL CCK-8 reagent per well and measured by a microplate reader (Thermo Scientific, USA). HUVECs and L929 were cultured in 12-well plates (3000 cells per well) for immunofluorescent staining. Please refer to supplementary document to check



Scheme 1. Schematic illustration of the inhibition process of tFNAs-Ery in *E. coli*. tFNAs increase the erythromycin efficiency by delivering it more inside the cells.

Table 1
Base Sequences of Each Specific ssDNA.

ss DNA	Base sequence (5'→3')
S1	ATTTATCACCGCCATAGTAGACGTATCACAGGCAGTTGAGACGAACATTCCTAAGTCTGAA
S2	ACATGCGAGGGTCCAATACCGACGATTACAGCTTGCTACACGATTACAGACTTAGGAATGTTCCG
S3	ACTACTATGGCGGGTGATAAAACGTGTAGCAAGCTGTAATCGACGGGAAGAGCATGCCCATCC
S4	ACGGTATTGGACCCCTCGCATGACTCAACTGCCTGGTGATACGAGGATGGGCATGCTCTTCCCG

Table 2
Loading efficiency of Erythromycin into tFNAs.

Sample	Initial Erythromycin (μg)	Abs peak area/total peak area (%)	Loading Erythromycin (μg)	Loading Efficiency (%)
1	4000	47.34	1893.6	47.34
2	2000	61.85	1237	61.85
3	1000	81.34	813.4	81.34
4	500	83.65	418.25	83.65
5	250	79.32	198.3	79.32

the specific procedure.

2.4. Cultivation of the microorganism

The *Escherichia coli* (*E. coli*) strain (BNCC133264) was obtained from BeNa Culture Collection (Beijing, China). A bacteria colony was picked up using gunpoint and was dipped in 3 mL Luria-Bertani (LB, pH 7.4) medium, cultivated in no carbon dioxide incubator at 37 °C. A turbidimeter was used to measure the bacterial concentration after the *E. coli* cells were isolated by centrifugation (4000 rpm, 3 min) and rinsed with PBS buffer. Measuring the optical density at 600 nm ($\text{OD}_{600\text{nm}}$) to determine the bacterial content. All tools and utensils were sterilized by autoclaving at 120 °C for 30 min and ultraviolet disinfection for 60 min before experiment.

2.5. Antibacterial assay

In order to observe the effect of tFNAs on *E. coli* growth, the $\text{OD}_{600\text{nm}}$ of bacteria was observed after 24 h of co-culture with different concentrations of tFNAs (100–500 nM). The control group was the *E. coli* with no treatment. The *E. coli* were adjusted with an initial density of 5×10^5 CFU/mL to set up different experimental groups in the 96-well plates for the minimum inhibitory concentration (MIC) test. For detailed experimental procedures, please refer to supplementary document. The $\text{OD}_{600\text{nm}}$ values of each group was recorded from 0 to 24 h through an automated spectrophotometer (BioTek Instruments, USA) and was drawn as the growth curve. The $\text{OD}_{600\text{nm}}$ values of the erythromycin, ssDNA-Ery and tFNAs-Ery group were recorded at 24 h to compare the bacterial growth between groups. Sterile straws were used to absorb the diluted *E. coli* liquid from the 96 wells plate corresponding to drug concentration of $0.25 \times \text{MIC}_{\text{Ery}}$ and inoculate it on MHB agar plate into a 37 °C incubator for 24 h, for the enumeration by plate count.

2.6. The ability of tFNAs-Ery to penetrate the bacterial cell wall membrane into the *E. coli*

To observe the inside-bacterial localization of tFNAs and tFNAs-Ery, the confocal laser microscope (TCS SP8; Leica, Wetzlar, Germany) was performed to catch bacterial images. ssDNA, tFNAs and tFNAs-Ery modifying by Cyanine-5 (Cy5) were incubated with *E. coli* (5×10^5 CFU/mL) in LB liquid medium at 37 °C for 3 h. The strain was centrifuged and collected and stained with SYTO-9 dye for 15 min. It was resuspended in PBS after washing three times by PBS. To measure bacterial uptake rate of ssDNA, tFNAs and tFNAs-Ery, the *E. coli* strain (10 000 cells for each sample) was measured using flow cytometer (FC500

Beckman, IL USA) after centrifuged and collected and suspended in 500 μL of PBS.

2.7. Assessment of the leakage of cytoplasm

100 nM tFNAs, erythromycin and tFNAs-Ery were separately incubated with 5×10^5 CFU/mL *E. coli*. The control group was untreated *E. coli*. All the samples were centrifuged (4000 rpm, 5 min) and filtrated to obtain the supernatants after incubation at 37 °C for 3 h. Atomic absorption spectrometer (AAS; SpectrAA 220FS, VARIAN, America) was used to analyzed the concentration of $[\text{Na}^+]$ and $[\text{K}^+]$ inside the obtained supernatants. Subsequently, the supernatants were additionally subjected to the o-Nitrophenyl- β -D-Glucopyranosides (ONPG) test, which involved incubation with 4 mM ONPG (20 h, 37 °C) followed by measurement of the optical density at 420 nm ($\text{OD}_{420\text{nm}}$) in a 96-well plate through a microplate reader.

2.8. The morphological observation of *E. coli*

The *E. coli* treated by 100 nM tFNAs, erythromycin and tFNAs-Ery respectively were collected and isolated. AFM, Scanning Electron Microscopy (FEI, INSPECT F, USA) and TEM were used to observe the morphological changes of the *E. coli*. The AFM sample (a drop of bacteria solution) suspended in PBS was dripped on cleaved mica dried for 20 min before putting into the instrument. For SEM observation, the *E. coli* cells were fixed overnight in 4% paraformaldehyde at 4 °C, dehydrated with anhydrous ethanol concentration gradient and then dried in vacuum and were coated with gilded film with their surface. TEM samples (*E. coli* cells fixation dehydration) were prepared with firmware copper carrier mesh for observation.

2.9. Stability analysis of tFNAs and tFNAs-Ery

tFNAs (250 nM) and tFNAs -Ery was co-incubated cultivated with 10% FBS, HUVECs cell lysate and *E. coli* lysate, respectively. Gel electrophoresis was used to observe the change of band for the nanostructure of tFNAs at 0–24 h.

2.10. Data analysis

SPSS 19.0 (IBM, Armonk, NY) was used for data analysis. ANOVA and *t*-test were conducted to obtain variance between-group. All quantitative results were presented as mean \pm standard deviation (SD). If the two-tailed P value was $<0.05^*$, $<0.01^{**}$, and $<0.001^{***}$, it can be considered that the data were significantly different.

3. Results

3.1. Characterization of tFNAs and tFNAs-Ery

8% polyacrylamide gel electrophoresis (PAGE), which was used to measure the molecular weight of tFNAs, showed that tFNAs is a self-assembled structure of four ssDNAs, each having a molecular weight of about 50 bp, while the tFNAs having a molecular weight of about 200 bp (Fig. 1b). Furthermore, atomic force microscopy (AFM) and transmission electron microscopy (TEM) demonstrated that tFNAs marked with dotted red line had a triangular shape, which is in accordance with

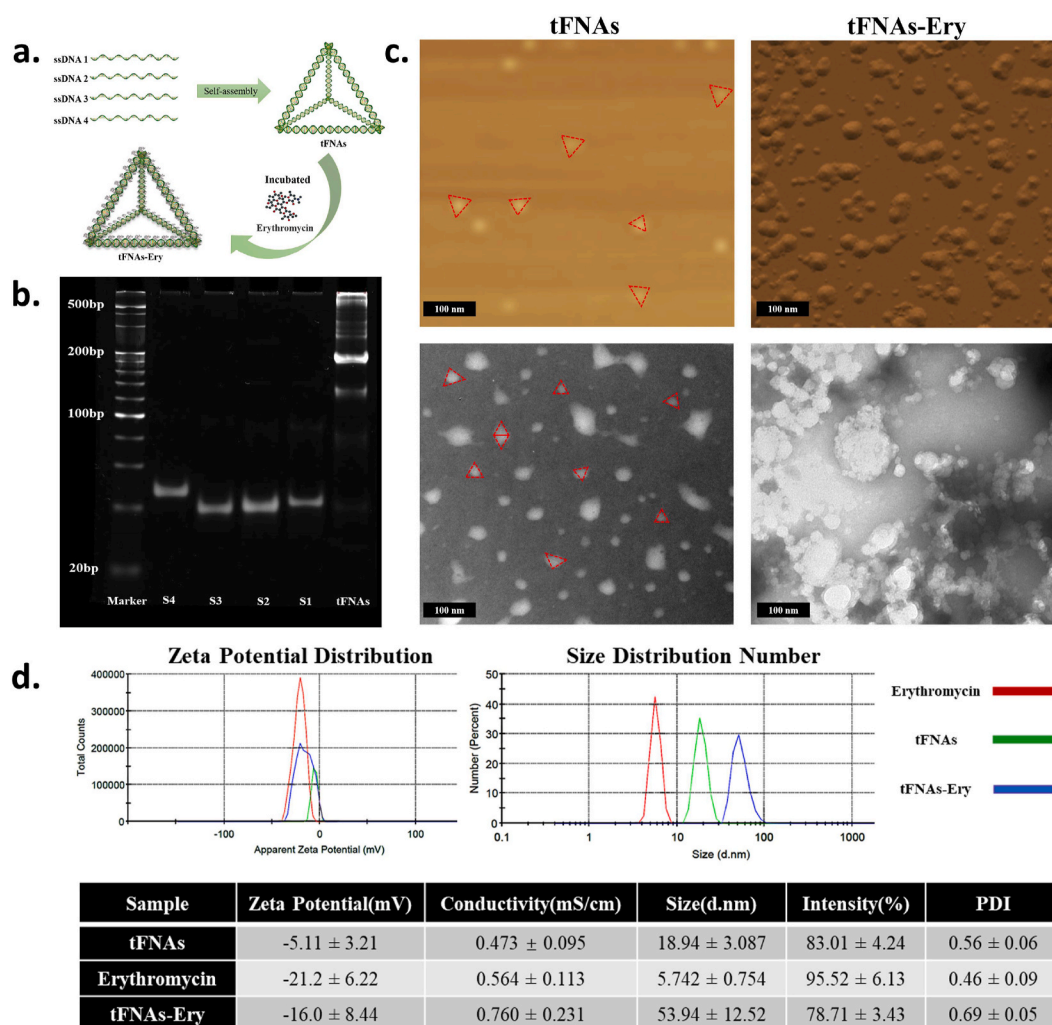


Fig. 1. Characterization of tFNAs and tFNAs-Ery. a. Schematic illustration synthesis of tFNAs-Ery. b. Confirmation of the successful synthesis of tFNAs by polyacrylamide gel electrophoresis (PAGE). The relative size of single-stranded DNA, partial assembly and tFNAs. c. Atomic Force Microscope Images and Transmission Electron Microscope Images of tFNAs (red dotted line) and tFNAs-Ery. d. Zeta potentials and Size of tFNAs and tFNAs-Ery. (For interpretation of the references to colour in this figure legend, the reader is referred to the Web version of this article.)

previous studies, while tFNAs-Ery had small particles around and inside the tFNAs (Fig. 1c). The sizes and zeta potentials of the tFNAs, erythromycin alone and tFNAs-Ery were determined using dynamic light scattering (DLS). The average zeta potential of tFNAs-Ery changed from -5.11 ± 3.21 mV to -16.0 ± 8.44 mV as the tFNAs was loaded with increasing amounts of erythromycin. The average size of tFNAs was 18.94 ± 3.087 nm, while that of tFNAs-Ery was 53.94 ± 12.52 nm (Fig. 1d). The results above highlight the convenience and efficiency of fabricating the tFNAs-Ery complex.

3.2. The biocompatibility of tFNAs and tFNAs-Ery

The cytotoxicity of tFNAs and tFNAs-Ery is an important consideration for further biological applications. Fig. 2a shows that even at a high dose (750 nM tFNAs; 500 μ g/mL tFNAs-Ery), tFNAs and tFNAs-Ery showed no obvious HUVEC cytotoxicity after incubation for 24 h and 48 h. On the other hand, growth inhibition in L929 cells were observed at 750 nM and 500 μ g/mL of tFNAs and tFNAs-Ery, respectively (Fig. 2c). To investigate the effect of tFNAs and tFNAs-Ery on the maintenance of HUVEC and L929 integrities, cell morphologies were investigated via immunofluorescent staining. Fig. 2b and d shows that the HUVEC and L929 cells exposed to tFNAs and tFNAs-Ery maintained normal cellular morphologies and showed normal cell proliferation. Notably, these

results suggested that 0–500 nM of tFNAs and 0–50 μ g/mL of tFNAs-Ery are safe for further in vivo use.

3.3. Determination of antibacterial activity in vitro

The optical density of *E. coli* at 600 nm (representing the density of bacteria) was measured after 24 h of incubation with erythromycin, ssDNA-Ery, and tFNAs-Ery, respectively. As shown in Fig. 3a, tFNAs-Ery showed a better antibacterial effect compared to erythromycin and ssDNA-Ery, based on MIC results. 0–300 nM of tFNAs had no significant effect on the growth of *E. coli* (Fig. 3b). The MIC of the erythromycin on *E. coli* is denoted as MIC_{Ery} and the MIC of tFNAs-Ery was a quarter of MIC_{Ery}. The OD_{600nm} value of different groups as the concentration of the erythromycin changes from $1 \times$ MIC_{Ery} to $0.25 \times$ MIC_{Ery} as showed in Fig. 3c. The density of bacteria of tFNAs-Ery group was significantly less than that of erythromycin group and ssDNA-Ery group at $0.5 \times$ MIC_{Ery} and $0.25 \times$ MIC_{Ery}. In groups treated with the same erythromycin treatment concentration, 24-h *E. coli* growth curves revealed that tFNAs-Ery had suppressed *E. coli* growth more than ssDNA-Ery and erythromycin (Fig. 3d). The CFU counts also demonstrated the above results (Fig. 3e). The plate colony count of the erythromycin and ssDNA-Ery treatment group had more colonies than those of tFNAs-Ery group through intuitive observation. The above results indicated that

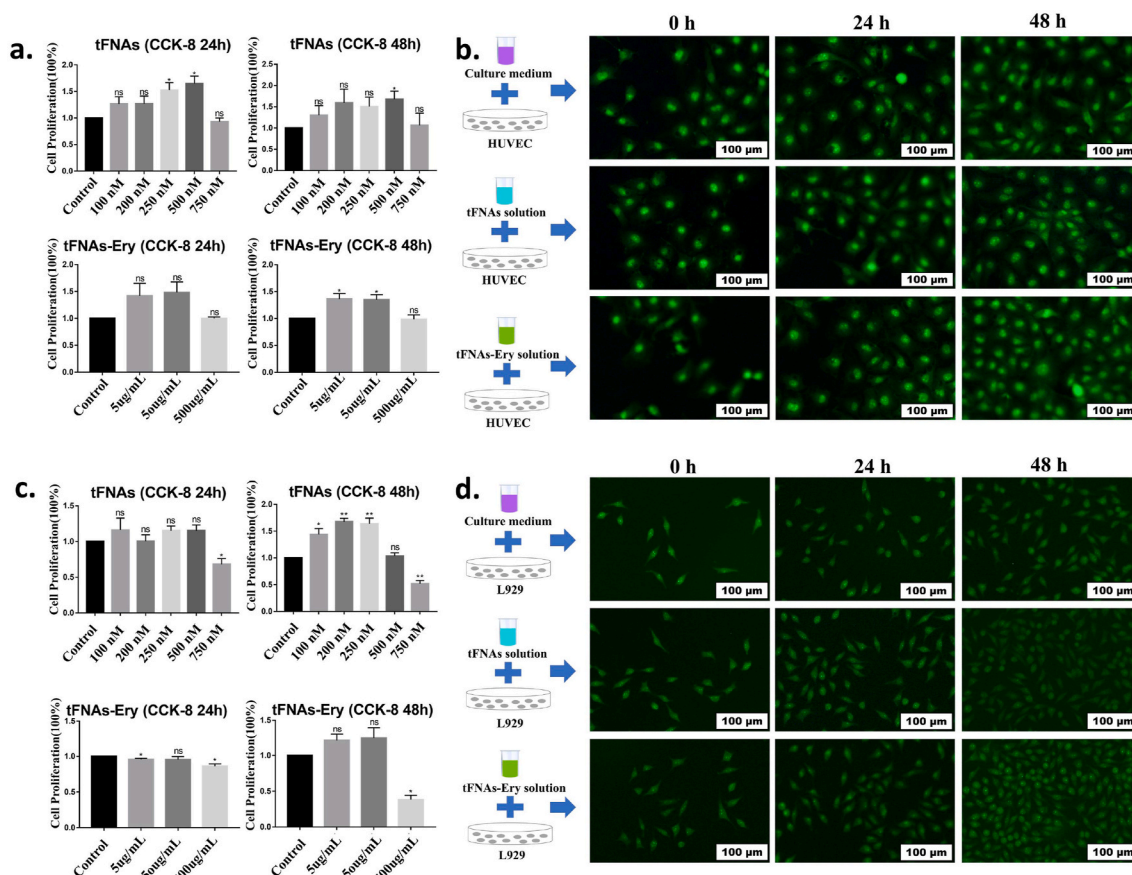


Fig. 2. Cytotoxicity test of tFNAs and tFNAs-Ery. a. HUVEC cells proliferation analyzed by CCK-8 assay after being cocultured with tFNAs and tFNAs-Ery at 24 h and 48 h. Statistical analysis ($n = 4$): *, $p < 0.05$; **, $p < 0.01$. b. Observation of HUVEC morphological changes after exposure to tFNAs and tFNAs-Ery by fluorescent microscopy. c. L929 cells proliferation analyzed by CCK-8 assay after being cocultured with tFNAs and tFNAs-Ery at 24 h and 48 h. Statistical analysis ($n = 4$): *, $p < 0.05$; **, $p < 0.01$. d. Observation of L929 morphological changes after exposure to tFNAs and tFNAs-Ery by fluorescent microscopy.

erythromycin has a better effect with the aid of tFNAs but ssDNA didn't work.

3.4. Bacterial uptake of tFNAs and tFNAs-Ery

Since erythromycin needs to enter the bacterial cell to manifest its bactericidal effect, the bacterial uptake of erythromycin is a mandatory first step for its mechanism of action. To determine whether tFNAs could successfully transport erythromycin inside *E. coli* cells, we tested the bacterial uptake of tFNAs and tFNAs-Ery via flow cytometry and confocal laser scanning microscopy (CLSM). As shown in Fig. 4a, untreated bacteria showed green fluorescence after incubation with SYTO-9, whereas Cy-5-labeled tFNAs and tFNAs-Ery showed red fluorescence. Therefore, obvious bacterial uptake of the fluorescent tFNAs or tFNAs-Ery appeared yellow in merged images. The CLSM images, which were consistent with the flow cytometry results, showed that the uptake ratio of tFNAs-Ery was more than that of tFNAs alone. Flow cytometry showed that the *E. coli* cellular uptake of Cy5-labeled tFNAs reached about 41.7% in 90 min, while Cy5-labeled tFNAs-Ery reached up to 90.6%. However, Cy-5-labeled ssDNA had difficulty in entering *E. coli* cells (Fig. 4c). Under the same drug concentration, tFNAs itself had no antibacterial effect, while tFNAs-Ery had a stronger antibacterial effect than erythromycin alone. These indicate that the tFNAs helped increase the concentration of erythromycin inside the target cells.

3.5. Stability analysis of tFNAs and tFNAs-Ery

According to the above results, we found that the tetrahedral spatial

structure of tFNAs is the key to its ability to efficiently carry erythromycin into the *E. coli* cells. Although the effective concentration of free erythromycin against *E. coli* is 20 $\mu\text{g}/\text{mL}$, our results demonstrated that even 5 $\mu\text{g}/\text{mL}$ of tFNAs-Ery was evidently bactericidally effective for 24 h. It is expected that tFNAs will remain structurally stable in the environment where bacteria grow and metabolize, and that their transport efficiency will not be reduced. To analyze the stability of tFNAs and tFNAs-Ery, we incubated tFNAs (250 nM) with 10% FBS, cell (HUVECs) lysate and *E. coli* lysate, respectively. Gel electrophoresis showed that the band for the tFNAs nanostructure remained almost unchanged after 12 h of incubation in 10% FBS, cell lysate and *E. coli* lysate, respectively (Fig. 4b). Furthermore, the band for the tFNAs could still be observed with a slightly attenuated intensity even after 24 h of incubation. These results indicate that tFNAs may be stable against nuclease degradation in biological media.

3.6. Morphological observation of *E. coli* cells

After the confirmation of the increased uptake of tFNAs-Ery by *E. coli* cells, individual cellular morphology was observed. The AFM images demonstrated that tFNAs alone caused little membrane changes, and erythromycin alone caused membrane deformation in *E. coli* cells. On the other hand, tFNAs-Ery caused the most serious membrane deformation, as demonstrated by the presence of debris, and break-off fragments. The SEM images revealed that the *E. coli* cells shrunk and formed more pores after receiving tFNAs-Ery, as compared with cells treated with erythromycin alone. Moreover, there was no difference between the tFNAs group and the control group. The TEM micrographs

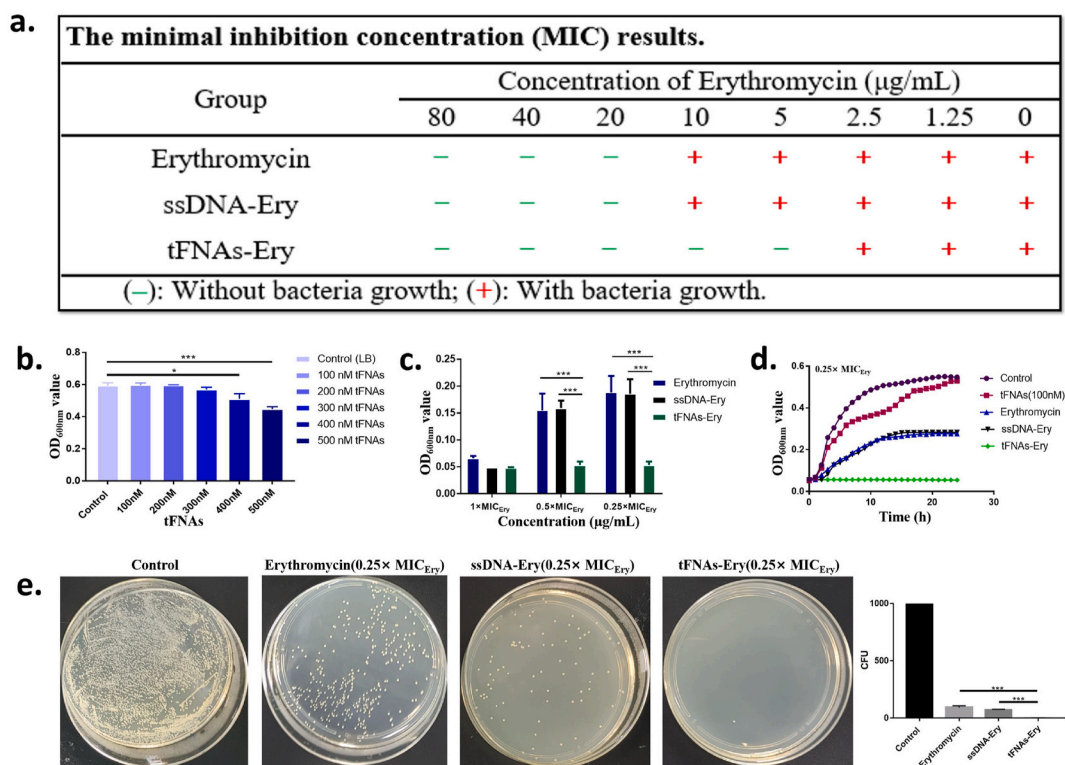


Fig. 3. Antibacterial activity of tFNAs-Ery on *E. coli*. a. The minimal inhibition concentration (MIC) results of erythromycin, ssDNA-Ery and tFNAs-Ery. b. The effect of different concentration of tFNAs on *E. coli* proliferation. The control group was the *E. coli* with no treatment. Statistical analysis ($n = 3$): *, $p < 0.05$; **, $p < 0.01$; ***, $p < 0.001$. c. Comparison of the antibacterial effects of erythromycin, ssDNA-Ery and tFNAs-Ery at $1 \times \text{MIC}_{\text{Ery}}$, $0.5 \times \text{MIC}_{\text{Ery}}$, $0.25 \times \text{MIC}_{\text{Ery}}$ by OD_{600nm} values. Statistical analysis ($n = 3$): *, $p < 0.05$; **, $p < 0.01$; ***, $p < 0.001$. d. The 24-h growth curves of *E. coli* after treating by 100nM tFNAs, $0.25 \times \text{MIC}_{\text{Ery}}$ of erythromycin, ssDNA-Ery and tFNAs-Ery. The control group was the *E. coli* with no treatment. e. Comparison of the plate colony count of *E. coli* in erythromycin, ssDNA-Ery and tFNAs-Ery groups at $0.25 \times \text{MIC}_{\text{Ery}}$.

demonstrated more details of the cytoplasm of *E. coli* cells treated with tFNAs-Ery (Fig. 5a).

3.7. Assessment of the leakage of cytoplasm

Based on the pore formation and cell shrinkage observed above, cytoplasm leakage and cell permeability were further assessed. β -galactosidase, an enzyme which can turn o-Nitrophenyl- β -D-Glucopyranosides (ONPG) into o-nitrophenol, a yellow product, is found in the normally impermeable *E. coli* cytoplasm. An increase in leakage indicates an increased membrane permeability, which can be quantitatively measured via the ONPG test. It was demonstrated that tFNAs-Ery led to a higher galactosidase leakage than erythromycin alone (Fig. 5b). Measuring the changes in intracellular $[\text{K}^+]$ and $[\text{Na}^+]$ is another strategy for quantitatively assessing the leakage and evaluating permeability, since a suitable content of $[\text{K}^+]$ concentration is necessary for *E. coli* survival. Consistent with the ONPG test, the tFNAs-Ery treatment led to a higher leakage of $[\text{K}^+]$ from *E. coli* cells than treatment with erythromycin alone. In addition, compared with the control group, the tFNAs-Ery treatment led to more changes in the $[\text{Na}^+]$ concentration than erythromycin alone (Fig. 5c).

4. Discussion

With the rapid development of DNA nanotechnology, a variety of self-assembled DNA nanomaterial with different sizes and spatial structures have been developed. The list of applications of DNA nanostructure research is endless in the field of molecular biology, including the use of these nanomaterials as biosensors, vehicles, for drug delivery, and so on [29–37]. At present, the antibacterial application of DNA nanostructures mainly focused on optimizing bactericidal performance

and cytotoxicity by combining these nanostructures with other antibacterial substances [38–41]. However, few studies have used DNA nanomaterials as transport carriers of commonly used antibiotics to address a certain degree of bacterial resistance. The most significant characteristic of gram-negative bacteria, such as *E. coli*, is their cell membrane composition, which includes an inner membrane, a watery periplasm containing a peptidoglycan layer, and an outer membrane. It is precisely because of the particularity of these structures that most antibiotics have difficulty crossing the bacterial cell membrane to produce an antibacterial effect. In addition, gram-negative bacteria also have efflux pumps, and drug sensors that can promote drug exit and monitor drug entry into the cell, respectively. Thus, it is very difficult to develop effective drugs against gram-negative bacteria [42–47]. Nanomaterials are gradually playing more important roles in antimicrobial studies, and many researchers have obtained valuable results. F. Nassar et al. developed a new uracil derivative and tested its antibacterial, antioxidant and anticancer activities. They found that the material was more effective against gram-positive bacteria than the control drug, cefoperazone. It also has high antibacterial activity against gram-negative bacteria [48]. Jin Hyunyeom and other researchers [49] used gold nanoparticles and DNA aptamers that bind to antimicrobial peptides and efficiently transfer them into mammalian cells. The use of these nanoparticles improves not only the stability of antimicrobial peptides, but also their effectiveness. Xiangyuan Ouyang et al. [50] had constructed a DNA nanoribbon with a width of 16 nm that was found to be a novel clinically relevant metallo- β -lactamase. Their discoveries provided a new platform for designing macromolecular inhibitors combined with β -lactam antibiotics against multidrug-resistant bacteria. In general, the combination of DNA nanostructures and antibiotics may be another promising research direction in the future. In our study, tFNAs-Ery were active against *E. coli* that are less sensitive to

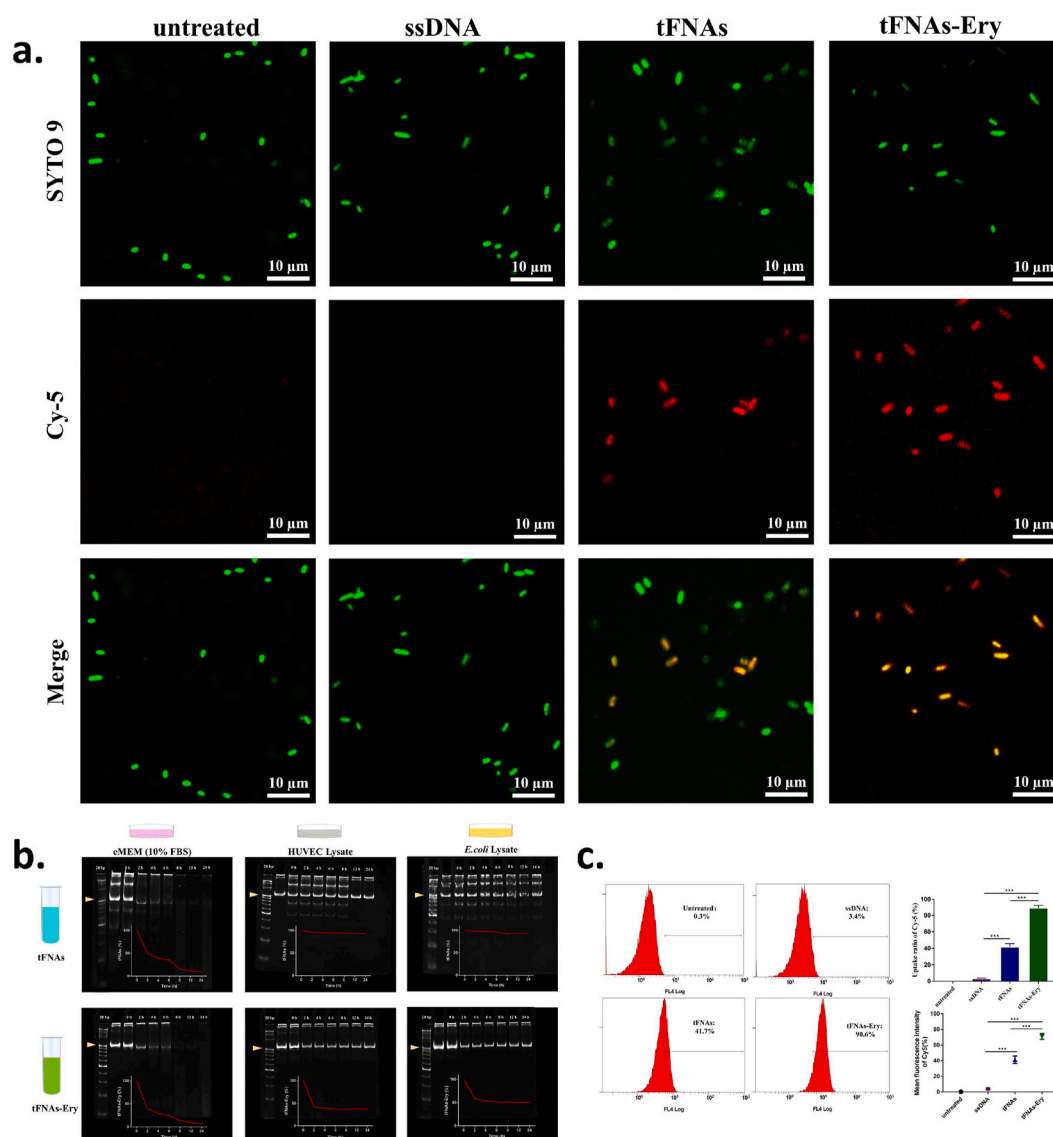


Fig. 4. The bacterial uptake and stability of tFNAs and tFNAs-Ery. a. Confocal laser scanning microscopy images of bacterial uptake of tFNAs and tFNAs-Ery in *E. coli* at 90 min. Green fluorescence shows the total number of live bacteria; Red fluorescence come from Cy5-ssDNA, Cy5-tFNAs or Cy5-tFNAs-Ery; Yellow fluorescence in the merge images represent Cy5-ssDNA, Cy5-tFNAs or Cy5-tFNAs-Ery co-located with the *E. coli*; Statistical analysis (n = 3): ***, p < 0.001. b. polyacrylamide gel electrophoresis (PAGE) analysis of the stability of tFNAs and tFNAs-Ery nanostructure after incubation with eMEM medium (with 10% FBS), HUVEC lysate (Protein concentration:500 μg/mL) and *E. coli* lysate (Protein concentration:500 μg/mL) at 37 °C for 0–24 h, respectively. c. Flow cytometry analysis of the uptake rates of *E. coli* incubated with ssDNA, tFNAs and tFNAs-Ery. The control group was the *E. coli* with no treatment; Statistical analysis (n = 3): ***, p < 0.001. (For interpretation of the references to colour in this figure legend, the reader is referred to the Web version of this article.)

erythromycin alone, they displayed a better in vitro antibacterial effectivity compared to erythromycin alone, a strong stability in the humoral environment, high bacteria-permeating ability and low resistance development. tFNAs-Ery is not a new antibiotic, it is a revised version of erythromycin, which restored the potency of the antibiotic. This makes the use of tFNAs an interesting and a useful strategy for future studies on antibiotic delivery.

5. Conclusion

In conclusion, we utilized tFNAs as a delivery platform for erythromycin. Our results demonstrated that tFNAs can enhance the antibacterial effects of erythromycin against *E. coli* as a result of an increased bacterial uptake. The reason for the increased bacterial uptake may be the augmentation of the permeability of microbial membranes due to interactions with tFNAs. Furthermore, tFNAs-Ery was stable in the

simulated bacterial internal environment in the first 8 h. Studies on the application of tFNAs delivery on other antibiotics, as well as on its effectivity against other types of bacteria, should be pursued in the future. In the development of tFNAs, the existing analysis focuses on its drug carrying capacity to improve the local concentration of antibiotics. Future studies should look into directly eradicating drug-resistant bacteria and reducing the MIC of antibiotics at the genetic level by designing special aptamers. The use of nucleic acid technology can inhibit or up-regulate the expression of specific genes, which may lead to alterations in bacterial growth and metabolism upon exposure to antibiotics.

Funding

This study was funded by the National Key R&D Program of China [2019YFA0110600] and National Natural Science Foundation of China

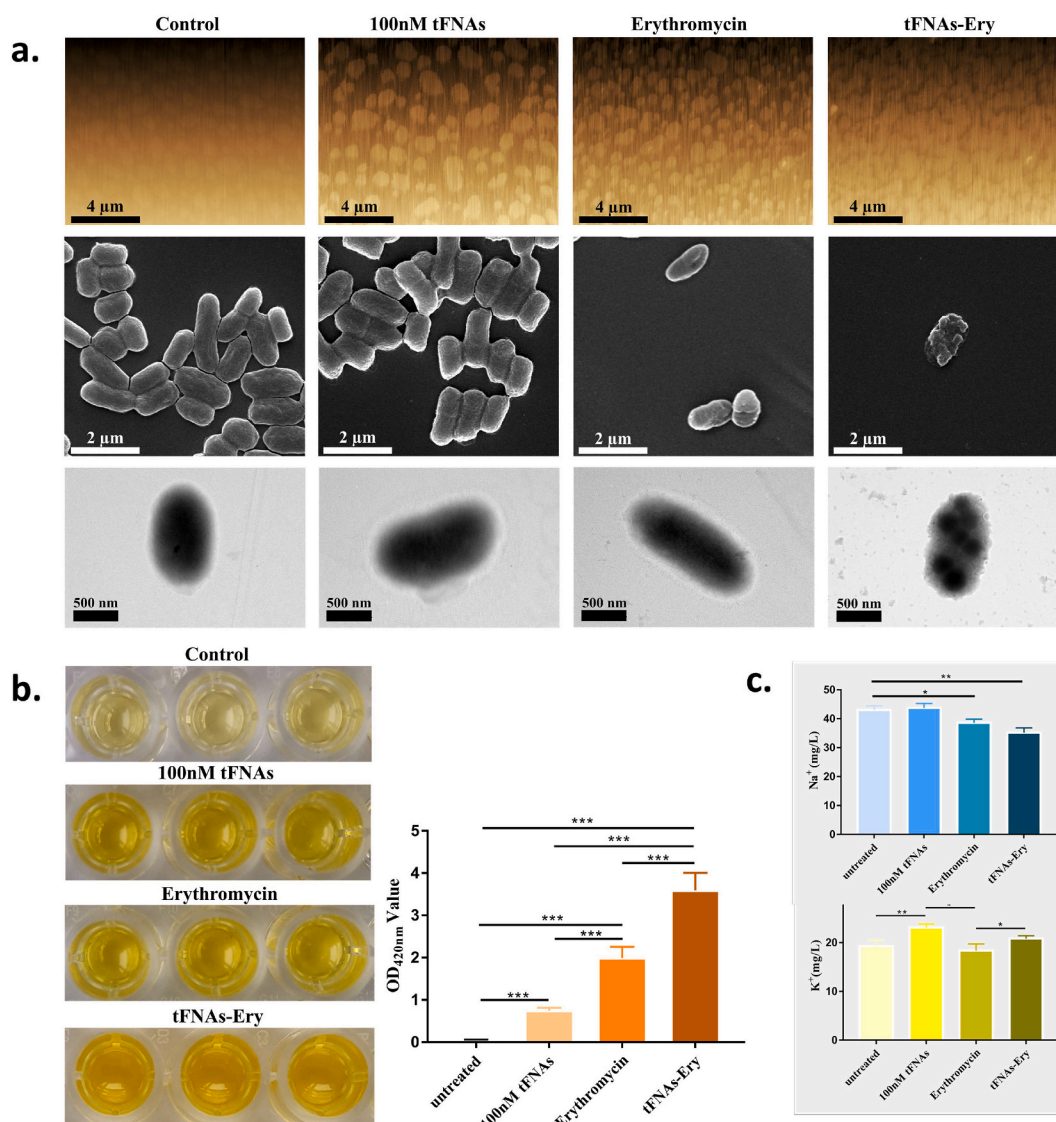


Fig. 5. Morphological changes and the leakage of cytoplasm. a. AFM, SEM and TEM images of *E. coli* after treatment with 100 nM tFNAs, erythromycin and tFNAs-Ery. The control group was the *E. coli* with no treatment. b. Leakage of β -galactosidase manifested by OD_{420nm} values of the supernatants of *E. coli* treated by 100 nM tFNAs, erythromycin and tFNAs-Ery. Statistical analysis ($n = 3$): *, $p < 0.05$; **, $p < 0.01$. c. Relative values of $[K^+]$ and $[Na^+]$ concentration of the supernatants of *E. coli* treated by 100 nM tFNAs, erythromycin and tFNAs-Ery, measured by AAS. Statistical analysis ($n = 3$): *, $p < 0.05$; **, $p < 0.01$.

[81970916, 81671031].

Data statement

The data that support the findings of this study are available from the corresponding author upon reasonable request.

CRediT authorship contribution statement

Yue Sun: Conceptualization, Investigation, Methodology, Project administration, Writing - original draft. **Yuhao Liu:** Data curation, Formal analysis, Investigation, Writing - review & editing. **Bowen Zhang:** Methodology, Investigation, Software. **Shirong Shi:** Data curation, Methodology, Resources. **Tao Zhang:** Data curation, Investigation, Writing - review & editing. **Dan Zhao:** Data curation, Methodology, Software. **Taoran Tian:** Resources, Methodology, Writing - review & editing. **Qirong Li:** Writing - review & editing. **Yunfeng Lin:** Project administration, Funding acquisition, Supervision, Writing - review & editing.

Declaration of competing interest

There is no conflict to declare.

Appendix A. Supplementary data

Supplementary data to this article can be found online at <https://doi.org/10.1016/j.bioactmat.2020.12.027>.

References

- [1] I.B. Seiple, Z. Zhang, P. Jakubec, A. Langlois-Mercier, P.M. Wright, D.T. Hog, K. Yabu, S.R. Allu, T. Fukuzaki, P.N. Carlsen, Y. Kitamura, X. Zhou, M.L. Condakes, F.T. Szczypiński, W.D. Green, A.G. Myers, A platform for the discovery of new macrolide antibiotics, *Nature* 533 (7603) (2016) 338–345, <https://doi.org/10.1038/nature17967>.
- [2] W. Cui, S. Ma, Recent advances in the field of 16-membered macrolide antibiotics, *Mini Rev. Med. Chem.* 11 (12) (2011) 1009–1018, <https://doi.org/10.2174/138955711797247734>.
- [3] R.I. Aminov, A brief history of the antibiotic era: lessons learned and challenges for the future, *Front. Microbiol.* 1 (2010) 134, <https://doi.org/10.3389/fmicb.2010.00134>.

- [4] M. Veerapandian, K. Yun, Functionalization of biomolecules on nanoparticles: specialized for antibacterial applications, *Appl. Microbiol. Biotechnol.* 90 (5) (2011) 1655–1667, <https://doi.org/10.1007/s00253-011-3291-6>.
- [5] G.P. Dinos, The macrolide antibiotic renaissance, *Br. J. Pharmacol.* 174 (18) (2017).
- [6] A. Biljana, B. Jili, Č. Ana, M. Milan, S. Nevena, N. Predrag, 16-membered macrolide antibiotics: a review, *Int. J. Antimicrob. Agents* 51 (3) (2018).
- [7] P. Laurent, J. Aurélie, N. Patrice Polymyxins, Antibacterial activity, susceptibility testing, and resistance mechanisms encoded by plasmids or chromosomes, *Clin. Microbiol. Rev.* 30 (2) (2017).
- [8] L. Mohanam, L. Priya, E.M. Selvam, S.S. Shivekar, T. Menon, Molecular mechanisms of efflux pump mediated resistance in clinical isolates of multidrug resistant *Pseudomonas aeruginosa*, *Int. J. Infect. Dis.* 45 (2016).
- [9] A. Lim, B. Naidenov, H. Bates, K. Willyerd, T. Snider, M.B. Couger, C. Chen, A. Ramachandran, Nanopore ultra-long read sequencing technology for antimicrobial resistance detection in *Mannheimia haemolytica*, *J. Microbiol. Methods* 159 (2019).
- [10] M. Lepoitevin, T. Ma, M. Bechelany, J.-M. Janot, S. Balme, Functionalization of single solid state nanopores to mimic biological ion channels: a review, *Adv. Colloid Interface Sci.* (2017) 250.
- [11] T. Zhang, T. Tian, R. Zhou, S. Li, W. Ma, Y. Zhang, N. Liu, S. Shi, Q. Li, X. Xie, Y. Ge, M. Liu, Q. Zhang, S. Lin, X. Cai, Y. Lin, Design, fabrication and applications of tetrahedral DNA nanostructure-based multifunctional complexes in drug delivery and biomedical treatment, *Nat. Protoc.* 15 (8) (2020) 2728–2757, <https://doi.org/10.1038/s41596-020-0355-z>.
- [12] J. Zhu, M. Zhang, Y. Gao, X. Qin, T. Zhang, W. Cui, C. Mao, D. Xiao, Y. Lin, Tetrahedral framework nucleic acids promote scarless healing of cutaneous wounds via the akt-signaling pathway, *Signal Transduct Targeted Thera* 5 (1) (2020) 120, <https://doi.org/10.1038/s41392-020-0173-3>.
- [13] S. Li, T. Tian, T. Zhang, X. Cai, Y. Lin, Advances in biological applications of self-assembled DNA tetrahedral nanostructures, *Mater. Today* 24 (2019) 57–68, <https://doi.org/10.1016/j.mattod.2018.08.002>.
- [14] Y. Liu, Y. Sun, S. Li, M. Liu, X. Qin, X. Chen, Y. Lin, Tetrahedral framework nucleic acids deliver antimicrobial peptides with improved effects and less susceptibility to bacterial degradation, *Nano Lett.* 20 (5) (2020) 3602–3610, <https://doi.org/10.1021/acs.nanolett.0c00529>.
- [15] Y. Zhang, X. Xie, W. Ma, Y. Zhan, C. Mao, X. Shao, Y. Lin, Multi-targeted antisense oligonucleotide delivery by a framework nucleic acid for inhibiting biofilm formation and virulence, *Nano-Micro Lett.* 12 (6) (2020) 117–129.
- [16] S. Strong, C. Yang, T. Taoran, L. Songhang, L. Shiyu, Z. Yuxin, S. Xiaoru, Z. Tao, L. Yunfeng, C. Xiaoxiao, Effects of tetrahedral framework nucleic acid/wogonin complexes on osteoarthritis, *Bone Res* 8 (2020) 6, <https://doi.org/10.1038/s41413-019-0077-4>.
- [17] Y. Zhan, W. Ma, Y. Zhang, C. Mao, X. Shao, X. Xie, F. Wang, X. Liu, Q. Li, Y. Lin, DNA-based nanomedicine with targeting and enhancement of therapeutic efficacy of breast cancer cells, *ACS Appl. Mater. Interfaces* 11 (17) (2019) 15354–15365, <https://doi.org/10.1021/acsami.9b03449>.
- [18] M. Liu, W. Ma, Q. Li, D. Zhao, X. Shao, Q. Huang, L. Hao, Y. Lin, Aptamer-targeted DNA nanostructures with doxorubicin to treat protein tyrosine kinase 7-positive tumours, *Cell Prolif* 52 (1) (2019) e12511, <https://doi.org/10.1111/cpr.12511>.
- [19] W. Ma, Y. Zhan, Y. Zhang, X. Xie, C. Mao, Y. Lin, Enhanced neural regeneration with a concomitant treatment of framework nucleic acid and stem cells in spinal cord injury, *ACS Appl. Mater. Interfaces* 12 (2) (2020) 2095–2106, <https://doi.org/10.1021/acsami.9b19079>.
- [20] P. Panchal, E. Ogunsona, T. Mekonnen, Trends in advanced functional material applications of nanocellulose, *Processes* 7 (1) (2018).
- [21] W. Emma, L. Antoin, W. Aine, R. Fiona, The use of nanoparticles in anti-microbial materials and their characterization, *Analyst* 133 (7) (2008).
- [22] S. Hadiya, X. Liu, W. Abd El-Hammed, M. Elsabahy, S.A. Aly, Levofloxacin-loaded nanoparticles decrease emergence of fluoroquinolone resistance in *Escherichia coli*, *Microb. Drug Resist.* 24 (8) (2018) 1098–1107, <https://doi.org/10.1089/mdr.2017.0304>.
- [23] K. Bush, P. Courvalin, G. Dantas, J. Davies, B. Eisenstein, P. Huovinen, G.A. Jacoby, R. Kishony, B.N. Kreiswirth, E. Kutter, S.A. Lerner, S. Levy, K. Lewis, O. Lomovskaya, J.H. Miller, S. Mobashery, L.J. Piddock, S. Projan, C.M. Thomas, A. Tomasz, P.M. Tulkens, T.R. Walsh, J.D. Watson, J. Witkowski, W. Witte, G. Wright, P. Yeh, H.I. Zgurskaya, Tackling antibiotic resistance, *Nat. Rev. Microbiol.* 9 (12) (2011) 894–896, <https://doi.org/10.1038/nrmicro2693>.
- [24] K. Lewis, Platforms for antibiotic discovery, *Nat. Rev. Drug Discov.* 12 (5) (2013) 371–387, <https://doi.org/10.1038/nrd3975>.
- [25] H.A. Hemege, Nanomaterials for alternative antibacterial therapy, *Int. J. Nanomed.* 12 (2017) 8211–8225, <https://doi.org/10.2147/IJN.S132163>.
- [26] C. Mao, W. Pan, X. Shao, W. Ma, Y. Zhang, Y. Zhan, Y. Gao, Y. Lin, The clearance effect of tetrahedral DNA nanostructures on senescent human dermal fibroblasts, *ACS Appl. Mater. Interfaces* 11 (2) (2019) 1942–1950, <https://doi.org/10.1021/acsami.8b20530>.
- [27] W. Ma, X. Xie, X. Shao, Y. Zhang, C. Mao, Y. Zhan, D. Zhao, M. Liu, Q. Li, Y. Lin, Tetrahedral DNA nanostructures facilitate neural stem cell migration via activating rhoa/rock2 signalling pathway, *Cell Prolif* 51 (6) (2018), e12503, <https://doi.org/10.1111/cpr.12503>.
- [28] M. Lin, J. Wang, G. Zhou, J. Wang, N. Wu, J. Lu, J. Gao, X. Chen, J. Shi, X. Zuo, C. Fan, Programmable engineering of a biosensing interface with tetrahedral DNA nanostructures for ultrasensitive DNA detection, *Angew. Chem. Int. Ed. Engl.* 54 (7) (2015) 2151–2155, <https://doi.org/10.1002/anie.201410720>.
- [29] X. Nuli, L. Shiyuan, Y. Xiaohai, H. Xiaoxiao, H. Jin, W. Kemin, DNA tetrahedron nanostructures for biological applications: biosensors and drug delivery, *Analyst* 142 (18) (2017).
- [30] Y. Zhang, W. Ma, Y. Zhan, C. Mao, X. Shao, X. Xie, X. Wei, Y. Lin, Nucleic acids and analogs for bone regeneration, *Bone Res* 6 (2018) 37, <https://doi.org/10.1038/s41413-018-0042-7>.
- [31] A. Baelo, R. Levato, E. Julian, A. Crespo, J. Astola, J. Gavaldà, E. Engel, M. A. Mates-Timoneda, E. Torrents, Disassembling bacterial extracellular matrix with dnase-coated nanoparticles to enhance antibiotic delivery in biofilm infections, *J. Contr. Release* 209 (2015) 150–158, [https://doi.org/S0168-3659\(15\)00258-8](https://doi.org/S0168-3659(15)00258-8).
- [32] H. Sun, J. Chao, X. Zuo, S. Su, X. Liu, L. Yuwen, C. Fan, L. Wang, Gold nanoparticle-decorated mos2 nanosheets for simultaneous detection of ascorbic acid, dopamine and uric acid, *RSC Adv.* 4 (52) (2014) 27625–27629, <https://doi.org/10.1039/c4ra04046e>.
- [33] X. Li, X. Xie, Z. Ma, Q. Li, L. Liu, X. Hu, C. Liu, B. Li, H. Wang, N. Chen, C. Fan, H. Song, Programming niche accessibility and in vitro stemness with intercellular DNA reactions, *Adv. Mater.* 30 (46) (2018), e1804861, <https://doi.org/10.1002/adma.201804861>.
- [34] J. Li, S. Song, X. Liu, L. Wang, D. Pan, Q. Huang, Y. Zhao, C. Fan, Enzyme-based multi-component optical nanopores for sequence-specific detection of DNA hybridization, *Adv. Mater.* 20 (3) (2008) 497, <https://doi.org/10.1002/adma.200701918>.
- [35] K. Xing, X.G. Chen, C.S. Liu, D.S. Cha, H.J. Park, Oleoyl-chitosan nanoparticles inhibits *Escherichia coli* and *Staphylococcus aureus* by damaging the cell membrane and putative binding to extracellular or intracellular targets, *Int. J. Food Microbiol.* 132 (2–3) (2009) 127–133, <https://doi.org/10.1016/j.ijfoodmicro.2009.04.013>.
- [36] F. Perche, T. Le Gall, T. Montier, C. Pichon, J.M. Malinge, Cardiolipin-based lipopolyplex platform for the delivery of diverse nucleic acids into gram-negative bacteria, *Pharmaceuticals* 12 (2) (2019), <https://doi.org/10.3390/ph12020081>.
- [37] M.I. Setyawati, R.V. Kutty, C.Y. Tay, X. Yuan, J. Xie, D.T. Leong, Novel theranostic DNA nanoscaffolds for the simultaneous detection and killing of *Escherichia coli* and *Staphylococcus aureus*, *ACS Appl. Mater. Interfaces* 6 (24) (2014) 21822–21831, <https://doi.org/10.1021/am502591c>.
- [38] C.H. Salamanca, C.J. Yancey, Y. Roman, A.F. Davalos, G.R. Rivera, Application of nanoparticle technology to reduce the anti-microbial resistance through beta-lactam antibiotic-polymer inclusion nano-complex, *Pharmaceuticals* 11 (1) (2018), <https://doi.org/10.3390/ph11010019>.
- [39] Y. Ge, T. Tian, X. Shao, S. Lin, T. Zhang, Y. Lin, X. Cai, Pegylated protamine-based adsorbing improves the biological properties and stability of tetrahedral framework nucleic acids, *ACS Appl. Mater. Interfaces* 11 (31) (2019) 27588–27597, <https://doi.org/10.1021/acsami.9b09243>.
- [40] M. Zhang, J. Zhu, X. Qin, M. Zhou, X. Zhang, Y. Gao, T. Zhang, D. Xiao, W. Cui, X. Cai, Cardioprotection of tetrahedral DNA nanostructures in myocardial ischemia-reperfusion injury, *ACS Appl. Mater. Interfaces* 11 (34) (2019) 30631–30639, <https://doi.org/10.1021/acsami.9b10645>.
- [41] L. Meng, W. Ma, S. Lin, S. Shi, Y. Li, Y. Lin, Tetrahedral DNA nanostructure-delivered dnzyme for gene silencing to suppress cell growth, *ACS Appl. Mater. Interfaces* 11 (7) (2019) 6850–6857, <https://doi.org/10.1021/acsami.8b22444>.
- [42] E.J. Culp, N. Waglechner, W. Wang, A.A. Fiebig-Comyn, Y.P. Hsu, K. Koteva, D. Sychantha, B.K. Coombes, M.S. Van Nieuwenhze, Y.V. Brun, G.D. Wright, Evolution-guided discovery of antibiotics that inhibit peptidoglycan remodelling, *Nature* 578 (7796) (2020) 582–587, <https://doi.org/10.1038/s41586-020-1990-9>.
- [43] G. Caruso, Antibiotic resistance in *Escherichia coli* from farm livestock and related analytical methods: a review, *J. AOAC Int.* 101 (4) (2018) 916–922, <https://doi.org/10.5740/jaoacint.17-0445>.
- [44] N. Roth, A. Käsbohrer, S. Mayrhofer, U. Zitz, C. Hofacre, K.J. Domig, The application of antibiotics in broiler production and the resulting antibiotic resistance in *Escherichia coli*: a global overview, *Poultry Sci.* 98 (4) (2019) 1791–1804, <https://doi.org/10.3382/ps/pey539>.
- [45] E. Sgariglia, N. Aconiti Mandolini, M. Napoleoni, L. Medici, R. Fraticelli, M. Conquista, P. Gianfelici, M. Staffolani, S. Fischella, M. Capucella, M. Sargenti, G. Perugini, Antibiotic resistance pattern and virulence genes in avian pathogenic *Escherichia coli* (apec) from different breeding systems, *Vet. Ital.* 55 (1) (2019) 26–33, <https://doi.org/10.12834/VetIt.1617.8701.1>.
- [46] N. Palma, M.J. Pons, C. Gomes, J. Mateu, M. Riveros, W. García, J. Jacobs, C. García, T.J. Ochoa, J. Ruiz, Resistance to quinolones, cephalosporins and macrolides in *Escherichia coli* causing bacteremia in peruvian children, *J. Global Antimicrob. Res.* 11 (2017) 28–33, <https://doi.org/10.1016/j.jgar.2017.06.011>.
- [47] S.A. Baron, J.M. Rolain, Efflux pump inhibitor ccpp to rescue colistin susceptibility in mcr-1 plasmid-mediated colistin-resistant strains and gram-negative bacteria, *J. Antimicrob. Chemother.* 73 (7) (2018) 1862–1871, <https://doi.org/10.1093/jac/dky134>.
- [48] I.F. Nassar, A.F.E. Faragay, F.M. Abdelrazek, Z. Hamza, Synthesis of new uracil derivatives and their sugar hydrazones with potent antimicrobial, antioxidant and anticancer activities, *Nucleos Nucleot. Nucleic Acids* 1–20 (2020), <https://doi.org/10.1080/15257770.2020.1736300>.
- [49] J.H. Yeom, B. Lee, D. Kim, J.K. Lee, S. Kim, J. Bae, Y. Park, K. Lee, Gold nanoparticle-DNA aptamer conjugate-assisted delivery of antimicrobial peptide effectively eliminates intracellular salmonella enterica serovar typhimurium, *Biomaterials* 104 (2016) 43–51, <https://doi.org/10.1016/j.biomaterials.2016.07.009>.
- [50] X. Ouyang, Y.N. Chang, K.W. Yang, W.M. Wang, J.J. Bai, J.W. Wang, Y.J. Zhang, S. Y. Wang, B.B. Xie, L.L. Wang, A DNA nanoribbon as a potent inhibitor of metallo-

beta-lactamases, Chem. Commun. 53 (63) (2017) 8878–8881, <https://doi.org/10.1039/c7cc04483f>.